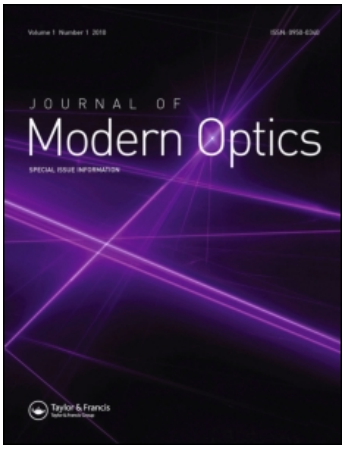


**Journal of Modern Optics**
Publication details, including instructions for authors and subscription information:
http://www.informaworld.com/smpp/title~content=t713191304

# Photonic Bands

Joseph W. Haus [ab]; H. Sami Sözüer [bc];Ramarao Inguva [c]
[a] Research Center for Advanced Science and Technology, The University of Tokyo, Tokyo, Japan [b] Physics Department, Rensselaer Polytechnic Institute, Troy, NY, U.S.A. [c] Department of Physics and Astronomy, University of Wyoming, Laramie, WY, USA

**To cite this Article** Haus, Joseph W. , Sözüer, H. Sami andInguva, Ramarao(1992) 'Photonic Bands', Journal of Modern Optics, 39: 10, 1991 — 2005
**To link to this Article: DOI:** 10.1080/09500349214552061
**URL:** http://dx.doi.org/10.1080/09500349214552061

JOURNAL OF MODERN OPTICS, 1992, VOL. 39, NO. 10, 1991–2005

# Photonic bands
## Ellipsoidal dielectric atoms in an f.c.c. lattice

JOSEPH W. HAUS†
Research Center for Advanced Science and Technology,
The University of Tokyo, 4-6-1 Komamba, Meguro-ku,
Tokyo 153, Japan

H. SAMI SÖZÜER† and RAMARAO INGUVA
Department of Physics and Astronomy,
University of Wyoming, Laramie, WY, 82071, USA

(*Received 3 December 1991; revision received 17 March 1992*)

**Abstract.** Photonic band structure has been computed using ellipsoidal grains in f.c.c. lattice. Bandgaps have been found and the conditions for the appearance of such gaps are discussed. The effective long-wavelength dielectric constants for the ordinary and the extraordinary rays are calculated and compared with the predictions of effective medium and Maxwell–Garnett theories.



## 1. Introduction

Photonic band structures in periodic heterogeneous materials have been generating broad interest in the scientific community [1–5]. The techniques are familiar from electronic band structure calculations but with important differences: the photonic band structure is calculated from a vector wave equation and the periodicity is imposed by known dielectric functions, instead of the rather complicated electronic potential which is usually replaced by an 'effective' one to facilitate computations. Defects can be introduced to create local modes and modify the density of states [6]. There are potential applications of these novel materials to controlled photon dispersion, improved semiconductor laser characteristics [7] and resonantly enhanced nonlinear optical effects [8]. Furthermore, fundamental properties can be examined, such as inhibited or enhanced spontaneous emission rates and quantum electrodynamics of atoms in these materials [9].

Photonic band structure determines important properties of the electromagnetic field, such as the density of states and the dispersion relations. When dielectric constants of the constituent components in the heterogeneous material differ by a substantial amount, a bandgap can emerge in which electromagnetic waves with frequencies within the gap are prohibited to exist and/or propagate within the material.

† Present address: Physics Department, Rensselaer Polytechnic Institute, Troy, NY 12180-3590, U.S.A.

0950-0340/92 $3·00 

The initial search for microstructures which were expected to possess a photonic bandgap concentrated on the face centred cubic (f.c.c.) lattice. Microstructures consisting of dielectric spheres embedded in a host of low dielectric constant and spherical voids within a dielectric material were examined. Experimental and computational efforts were focused on the second and third bands where a gap was expected. However, no 2–3 gap was found in these structures. The existence of a gap between the eighth and ninth bands has recently been shown by the authors [10] for spherical voids in f.c.c. Other attempts at finding a bandgap have used the diamond lattice [5] or gridlike structures [2, 15].

Even though the numerical techniques seem routine, care must be exercised in assuring convergence. When the dielectric function, and consequently the fields, are discontinuous, the results must be carefully examined before definitive conclusions can be drawn. In previous work [10, 11] we used two complementary methods to ensure convergence of the plane wave method. This approach is used in this paper as well.

We calculated the band structure for ellipsoidal atoms periodically arranged in an f.c.c. lattice. Ellipsoidal atoms are interesting in that they are birefrigent in the long-wavelength regime and the degeneracy at the $W$ point which prevents the lowest gap from forming is removed, although other accidental degeneracies may exist depending on the orientation and the aspect ratio of the ellipsoids. Such structures also provide an interesting test of the analytic theories for the long-wavelength dielectric tensor. Moreover, after examining the sensitive dependence of the band structure on the aspect ratio, orientation and the volume fraction of the ellipsoids, we conjecture that an important element in the emergence of the photonic bandgap is the connectedness of the dielectric components that make up the microstructure.

In previous work [10] we interpreted $\varepsilon(\mathbf{r})$ as the weight function and showed that its relative fluctuation from its spatial average provides a measure of deviation from the free photon problem. Writing $\varepsilon(\mathbf{r}) = \bar{\varepsilon}[1 + \varepsilon_r(\mathbf{r})]$, where $\bar{\varepsilon}$ is the spatial average of $\varepsilon(\mathbf{r})$, it is readily seen that $\bar{\varepsilon}$ is an overall scaling factor and $\|\varepsilon_r\| \equiv \|\varepsilon_{\text{fluc}}\|/\bar{\varepsilon}$ is a measure of the deviation from the free photon problem. We indeed find that when the r.m.s. fluctuation of $\varepsilon(\mathbf{r})$ becomes comparable to its spatial average, i.e. when $\|\varepsilon_r\| \simeq 1$, significant deviations from the free photon problem, such as bandgaps, begin to appear.

In what follows, we highlight the two methods and their rates of convergence. Later, we discuss the long wavelength limit and the accuracy of various theories when the ellipsoidal 'atoms' have a high volume fraction. Finally, we discuss the appearance of bandgaps with the reduced symmetry of the Brillouin zone taken into account. We conclude with remarks about conditions under which bandgaps emerge.

## 2. Method

We start with Maxwell's equations for $\mathscr{E}$ and $\mathscr{H}$ in a dielectric medium

$$\nabla \times \nabla \times \mathscr{E}(\mathbf{r}, t) + \frac{1}{c^2} \frac{\partial^2}{\partial t^2} \varepsilon(\mathbf{r}) \mathscr{E}(\mathbf{r}, t) = 0, \tag{1}$$

$$\nabla \times \eta(\mathbf{r}) \nabla \times \mathscr{H}(\mathbf{r}, t) + \frac{1}{c^2} \frac{\partial^2}{\partial t^2} \mathscr{H}(\mathbf{r}, t) = 0, \tag{2}$$

where $\eta(\mathbf{r}) \equiv 1/\varepsilon(\mathbf{r})$ and $\varepsilon(\mathbf{r})$ is linear, isotropic, positive-definite and periodic with lattice vectors $\mathbf{R}$

$$\varepsilon(\mathbf{r}) = \varepsilon(\mathbf{r}-\mathbf{R}) > 0. \tag{3}$$

The eigenfunctions of equations (1, 2) are Bloch functions of the form

$$\mathbf{E}_{n\mathbf{k}}(\mathbf{r}, t) = \exp[\mathrm{i}(\mathbf{k}\cdot\mathbf{r} - \omega_{n\mathbf{k}}t)] \sum_{\mathbf{G}} \mathbf{E}_{n\mathbf{k}}(\mathbf{G}) \exp[\mathrm{i}(\mathbf{G}\cdot\mathbf{r})]. \tag{4}$$

$$\mathbf{H}_{n\mathbf{k}}(\mathbf{r}, t) = \exp[\mathrm{i}(\mathbf{k}\cdot\mathbf{r} - \omega_{n\mathbf{k}}t)] \sum_{\mathbf{G}} \mathbf{H}_{n\mathbf{k}}(\mathbf{G}) \exp[\mathrm{i}(\mathbf{G}\cdot\mathbf{r})], \tag{5}$$

where $\mathbf{G}$ is a reciprocal lattice vector and the Fourier coefficients $\mathbf{E}_{\mathbf{G}} \equiv \mathbf{E}_{n\mathbf{k}}(\mathbf{G})$ and $\mathbf{H}_{\mathbf{G}}$ satisfy, respectively, the infinite-dimensional matrix equations

$$(\mathbf{k}+\mathbf{G}) \times (\mathbf{k}+\mathbf{G}) \times \mathbf{E}_{\mathbf{G}} + \frac{\omega^2}{c^2} \sum_{\mathbf{G}'} \varepsilon_{\mathbf{G}\mathbf{G}'} \mathbf{E}_{\mathbf{G}} = 0, \tag{6}$$

$$(\mathbf{k}+\mathbf{G}) \times \sum_{\mathbf{G}'} \eta_{\mathbf{G}\mathbf{G}'} (\mathbf{k}+\mathbf{G}') \times \mathbf{H}_{\mathbf{G}'} + \frac{\omega^2}{c^2} \mathbf{H}_{\mathbf{G}} = 0, \tag{7}$$

with $\varepsilon_{\mathbf{G}\mathbf{G}'} \equiv \varepsilon(\mathbf{G}-\mathbf{G}')$ and $\eta_{\mathbf{G}\mathbf{G}'} \equiv \eta(\mathbf{G}-\mathbf{G}')$. Equation (6) is an infinite-dimensional generalized Hermitian eigenproblem, hereafter referred to as the **E** method, while equation (7) is an ordinary one, which we will call the **H** method. The Bloch functions satisfy the following orthogonality relations [10]

$$\int_{\text{all r}} \mathrm{d}\mathbf{r} \exp[-\mathrm{i}(\mathbf{k}-\mathbf{k}')\cdot\mathbf{r}]\, \varepsilon(\mathbf{r}) \mathbf{E}^*_{n'}(\mathbf{r}) \cdot \mathbf{E}_{n\mathbf{k}}(\mathbf{r}) = C_{n\mathbf{k}} \delta_{nn'} \delta(\mathbf{k}-\mathbf{k}'), \tag{8}$$

$$\int_{\text{all r}} \mathrm{d}\mathbf{r} \exp[-\mathrm{i}(\mathbf{k}-\mathbf{k}')\cdot\mathbf{r}]\, \mathbf{H}^*_{n'\mathbf{k}'}(\mathbf{r}) \cdot \mathbf{H}_{n\mathbf{k}}(\mathbf{r}) = C'_{n\mathbf{k}} \delta_{nn'} \delta(\mathbf{k}-\mathbf{k}'), \tag{9}$$

where $\{C_{n\mathbf{k}}\}$ and $[C'_{n\mathbf{k}}]$ are real and positive normalization constants. It is important to note that the $\mathscr{E}$ field is normalized with $\varepsilon(\mathbf{r})$ as the weight function. The magnetic potential $\mathscr{A}$, which satisfies the same eigenvalue equation as $\mathscr{E}$ in the gauge where the scalar potential $\phi = 0$ (note that this is no longer the transverse gauge, as $\nabla \cdot \mathscr{A} \neq 0$), is also normalized with the same weight function. The normal modes of the electromagnetic field are no longer plane waves. The field Hamiltonian is

$$H \equiv \frac{1}{8\pi} \int_{\text{all r}} \mathrm{d}\mathbf{r} [\mathscr{E}\cdot\mathscr{D} + \mathscr{B}\cdot\mathscr{H}] \tag{10}$$

$$= \frac{1}{2\pi} \sum_n \int_{\text{BZ}} \mathrm{d}\mathbf{k} \left(\frac{\omega_{n\mathbf{k}}}{c}\right)^2 \sum_{\mathbf{G},\mathbf{G}'} \varepsilon(\mathbf{G}-\mathbf{G}') \mathbf{A}^*_{n\mathbf{k}}(\mathbf{G}) \cdot \mathbf{A}_{n\mathbf{k}}(\mathbf{G}'). \tag{11}$$

A proper second quantization [16] and the quantum electrodynamics of an atom in a periodic dielectric medium must start from this field Hamiltonian.

We have shown [10, 11] that although the two formulations, the **E** and the **H** method, would yield the same spectrum when an infinite number of plane waves are included, their truncated forms yield, in general, very different spectra even when as many as a few thousand plane waves are used.

Using $\nabla \cdot \nabla \times \mathscr{E} = 0$ and $\nabla \cdot \mathscr{H} = 0$, the $3N \times 3N$ matrix equations (6) and (7) can be cast into $2N \times 2N$ ordinary Hermitian forms which are computationally more efficient. Hence the **E** method is identical to the method of Ho *et al.* [5], while the **H** method uses the same matrix equation with $\tilde{\varepsilon}^{-1}_{\mathbf{GG}'}$ replaced by $\eta_{\mathbf{GG}'}$.

Following Zhang and Satpathy [4], one could also start with the equation satisfied by the $\mathscr{D}$ field

$$\nabla \times \nabla \times \eta(\mathbf{r})\mathscr{D}(\mathbf{r}, t) + \frac{1}{c^2}\frac{\partial^2}{\partial t^2}\mathscr{D}(\mathbf{r}, t) = 0. \tag{12}$$

This was shown to be completely equivalent to the **H** method [10].

The lowest-order Fourier expansion for each method yields the two possible extreme limits for the effective long-wavelength dielectric constant $\varepsilon_{\text{eff}}$. This gives the methods a complementary structure, since, as the number of plane waves used in the expansion is increased, they approach a common limit from two extreme starting points.

## 3. Ellipsoidal atoms

We consider in this paper ellipsoidal dielectric atoms.

$$\varepsilon(\mathbf{r}) = \varepsilon_b + \sum_{\mathbf{R}} \varepsilon_0(\mathbf{r} - \mathbf{R}). \tag{13}$$

$\varepsilon_b$ is the dielectric constant of the background and $\varepsilon_0(\mathbf{r} - \mathbf{R})$ is the contribution to the dielectric function at $\mathbf{r}$ from the **R**th 'atom'. We introduce the primed coordinate system in which the ellipsoids have the standard form

$$a_{ij} \equiv \hat{\mathbf{e}}'_i \cdot \hat{\mathbf{e}}_j. \tag{14}$$

For any vector **V**

$$\mathbf{V} = \sum_{j=1}^{3} V_j \hat{\mathbf{e}}_j = \sum_{i=1}^{3} V'_i \hat{\mathbf{e}}'_i, \tag{15}$$

$$V'_i = \sum_{j=1}^{3} a_{ij} V_j, \qquad V_j = \sum_{i=1}^{3} a_{ij} V'_i. \tag{16}$$

For notational convenience, we define

$$u \equiv \left[\sum_{i=1}^{3}\left(\frac{x'_i}{\sigma_i}\right)^2\right]^{1/2} \equiv u(\mathbf{r}), \tag{17}$$

$$g \equiv \left[\sum_{i=1}^{3}(G'_i\sigma_i)^2\right]^{1/2} \equiv g(\mathbf{G}). \tag{18}$$

where $\sigma_i$ are the principal axes of the ellipsoid and **G** is a reciprocal lattice vector. We refer to any function of $u$ as an 'ellipsoidally symmetric' function.

For $\varepsilon_0(\mathbf{r}) = \varepsilon_0[u(\mathbf{r})]$,

$$\varepsilon(\mathbf{r}) = \sum_{\mathbf{G}} \varepsilon(\mathbf{G}) \exp(i\mathbf{G} \cdot \mathbf{r}), \tag{19}$$

$$\begin{aligned}\varepsilon(\mathbf{G}) &= \frac{1}{V_{\text{cell}}}\int_{\text{WS cell}} d\mathbf{r} \exp(-i\mathbf{G} \cdot \mathbf{r})\,\varepsilon(\mathbf{r}) \\ &= \varepsilon_b \delta_{\mathbf{G0}} + \frac{4\pi\sigma_1\sigma_2\sigma_3}{gV_{\text{cell}}}\int_0^\infty du\, u \sin gu\, \varepsilon_0(u),\end{aligned} \tag{20}$$

where $V_{\text{cell}}$ is the volume of the primitive lattice cell and a similar result holds for the Fourier transform of $\eta(\mathbf{r})$.

To truncate the infinite-dimensional eigenvalue problem, a subset of $\{\mathbf{G}\}$ must be selected. For spherical atoms, symmetry dictates that this subset be all $\mathbf{G}$ points inside a sphere of radius $G_{max}$. The straightforward generalization of ellipsoidal atoms is the selection of $\mathbf{G}$ points inside the 'reciprocal ellipsoid' defined by

$$\{\mathbf{G}|g(\mathbf{G}) \leqslant g_{\max}\}, \tag{21}$$

where $g_{\max}$ is the 'radius' of the ellipsoid containing $N$ $\mathbf{G}$ points. The precise shape of this volume should be irrelevant as $N$ becomes larger and indeed we find that a spherical or an ellipsoidal truncation volume yields almost the same spectrum for large $N$ when convergence is good.

## 4. Spheroids

In what follows, unless otherwise noted, all lengths are in units of $a/2\pi$ and all wave-vectors $\mathbf{k}$, $\mathbf{G}$ are in units of $2\pi/a$, where $a$ is the side of the conventional cubic unit cell.

For a periodic array of dielectric spheroids, with principal axes $\sigma_1 = \sigma_2 = \sigma_{12}$ and $\sigma_3$ and dielectric constant $\varepsilon_a$, imbedded in a hose medium with $\varepsilon_b$,

$$\varepsilon(\mathbf{r}) = \varepsilon_b + (\varepsilon_a - \varepsilon_b) \sum_{\mathbf{R}} \theta[1 - u(\mathbf{r} - \mathbf{R})]. \tag{22}$$

Its Fourier transform is

$$\varepsilon(\mathbf{G}) = \varepsilon(g) = \varepsilon_b \delta_{\mathbf{G}0} + 3\beta(\varepsilon_a - \varepsilon_b) \frac{\sin g - g \cos g}{g^3}, \tag{23}$$

where $\beta$ is the volume packing fraction of the $\varepsilon_a$ material, and a similar expression is obtained for $\eta(\mathbf{G})$.

### 4.1. *The long-wavelength limit*

The long-wavelength limit is important from a practical as well as a theoretical point of view. The rich literature on the effective long-wavelength dielectric tensor, $\varepsilon_{\text{eff}}$, makes it possible to compare our results with various theories. This is an invaluable test since convergence is often, although not always, a serious problem. The lowest order estimate for $\varepsilon_{\text{eff}}$ obtained from the **E** and the **H** method are $\varepsilon(\mathbf{G} = \mathbf{0})$ and $1/\eta(\mathbf{G} = \mathbf{0})$, where $\varepsilon(\mathbf{G} = \mathbf{0})$ is the spatial average of $\varepsilon(\mathbf{r})$, and $\eta(\mathbf{G} = \mathbf{0})$ is that of $1/\varepsilon(\mathbf{r})$. The two quantities are quite different when the dielectric contrast is high. We have found that the rate of convergence of each method depends on the type of dielectric medium. However, we can generally conclude that the method whose lowest order approximation for $\varepsilon_{\text{eff}}$ is closer to the actual case will converge faster, although for certain topologies, convergence becomes an insurmountable problem with either method. Poor convergence in the long-wavelength limit implies poor convergence for the lowest two bands throughout the entire Brillouin zone, including its boundary. Hence, in order to have accurate estimates for the lowest gap one must have good convergence in this regime.

The effective long-wavelength dielectric constant for waves with a reduced wavevector $\mathbf{k} \equiv k\hat{\mathbf{k}}$, is defined as

$$\varepsilon_{\text{eff}-n}(\hat{\mathbf{k}}) \equiv \lim_{k \to 0} \frac{c^2}{|\mathrm{d}\omega_n(k\hat{\mathbf{k}})/\mathrm{d}k|^2}, \tag{24}$$

where $n = 1, 2$ is the polarization index and $\varepsilon_{\text{eff}-n}(\hat{\mathbf{k}})$ will, in general, be distinct for each $\hat{\mathbf{k}}$ for arbitrarily shaped atoms. For ellipsoidal atoms, $\varepsilon_{\text{eff}-n}(\hat{\mathbf{k}})$ defines ellipsoids normal in the primed coordinate system. For spheroidal atoms $\varepsilon_{\text{eff}-n}(\hat{\mathbf{k}})$ defines a sphere with radius $\varepsilon_{\text{eff}-O}$ for one polarization, and a spheroid with principal axes $\varepsilon_{\text{eff}-O}$ and $\varepsilon_{\text{eff}-X}$ for the other. We calculated $\varepsilon_{\text{eff}-O}$ and $\varepsilon_{\text{eff}-X}$ using the two lowest frequencies at $\mathbf{k} = 0{\cdot}05\hat{\mathbf{e}}'_1$.

Our calculations for $\varepsilon_{\text{eff}}$ are very close to the predictions of the Maxwell–Garnett theory for the host/guest topology, where dielectric atoms of one type are completely immersed in a background medium. It has been shown earlier that for air atoms the **E** method converges faster and for dielectric atoms the **H** method is better [10]. In figure 1, we plot $\varepsilon_{\text{eff}}$ against $N^{-1/3}$ for both the ordinary and the extraordinary rays calculated by both methods for air spheroids, $\varepsilon_a = 1$, $\varepsilon_b = 13$, $\sigma_1 = \sigma_2 = \pi/2$, $\sigma_3 = \pi$, with the symmetry axis of the spheroids in the (111) direction. It is quite clear that the convergence of the **E** method is excellent, and $\varepsilon_{\text{eff}}^{\mathbf{H}}$, when extrapolated to $N^{-1/3} \to 0$, yields consistent results, although it still has not converged. Figure 2 is a similar plot for dielectric spheroids in an air background. Although convergence of neither method is satisfactory, an extrapolation to $N^{-1/3} \to 0$ yields results within a few per cent of one another.

Figure 3 is a plot of $\varepsilon_{\text{eff}}$ for air spheroids, calculated by a simple linear extrapolation, for $\varepsilon_a = 13$, $\varepsilon_b = 1$, $\beta = 0{\cdot}5$ with the aspect ratio $\sigma_</\sigma_>$ varied. Also plotted are the Maxwell–Garnett [12] and the effective medium [13] results. Figure 4

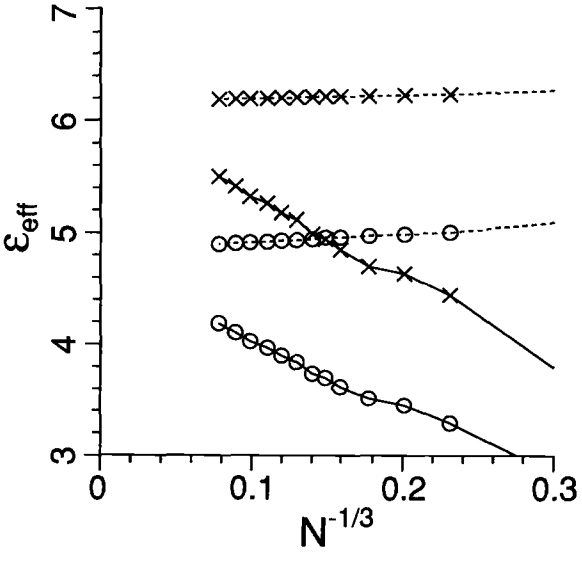


Figure 1. $\varepsilon_{\text{eff}-O}$ (○), and $\varepsilon_{\text{eff}-X}$ (×) against $N^{-1/3}$ for air spheroids oriented along the (111) direction in f.c.c. using the **E** method (dashed), and the **H** method (solid). $\varepsilon_b = 13$, $\varepsilon_a = 1$, and $\beta = \pi/6$.

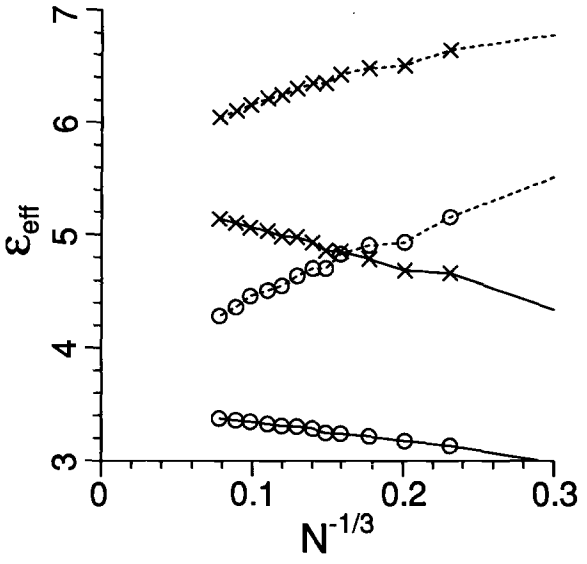


Figure 2. Same as figure 1 but for dielectric spheroids. $\varepsilon_b = 1$, $\varepsilon_a = 13$, and $\beta = \pi/6$.

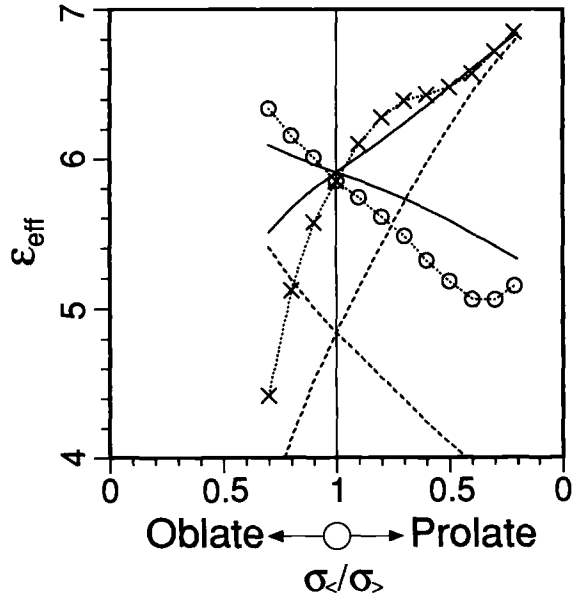


Figure 3. $\varepsilon_{eff-O}$ (○), and $\varepsilon_{eff-X}$ (×) against the aspect ratio for air spheroids oriented along the (111) direction in f.c.c. $\varepsilon_b = 13$, $\varepsilon_a = 1$, and $\beta = 0{\cdot}5$. The dashed curves are the predictions of the effective-medium theory, and the solid curves are predictions of the Maxwell–Garnett theory.

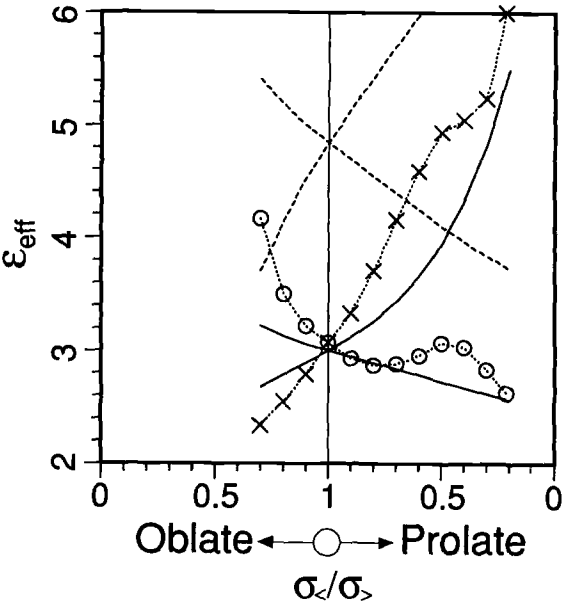


Figure 4. Same as figure 3 but for dielectric spheroids. $\varepsilon_b = 1$, $\varepsilon_a = 13$, and $\beta = 0{\cdot}5$.

is a similar plot for dielectric spheroids. The agreement with the Maxwell–Garnett results is not perfect due to proximity effects [14] which become increasingly significant as the aspect ratio decreases, since the volume fraction of the spheroids is quite high. For lower volume fractions, however, we find much better agreement with the Maxwell–Garnett theory.

The effective medium result, in which both types of materials appear on an equal footing, fails badly throughout. As has been pointed out earlier [10, 14], it does make a difference which type of material is the host and which one is the guest. The fields are radically different for the two cases in the quasistatic limit.

### 4.2. *The band structure*

We investigated the band structures of a variety of spheroidal atoms when the $z'$ axis of the spheroid lies along the (001), (110) and (111) directions for different volume fractions and eccentricities. We found the largest bandgaps for prolate air spheroids for $\sigma_3/\sigma_{12} = 2$, $\beta = \pi/6$ and with the symmetry axis along the (111) direction. When the spheroids 'overlap' the gaps are greatly increased. For dielectric spheroids in air with the same geometry, we failed to find gaps using either method. Although convergence is a serious problem with these structures, examining the results obtained from each method as $N$ is increased, we can safely say that there are no gaps. With the **E** method, there seems to be a small gap when a small number of plane waves are included, but these disappear as $N$ is increased. With the **H** method, we did not find gaps for $N$ up to about 1500. We also tried 'overlapping' dielectric spheroids, to be described below, and failed to find any gaps for these cases either, although there is almost certainly a 'direct transition gap', i.e. the second and third bands are never degenerate.

For spherical atoms in a lattice with cubic symmetry, there are 48 symmetry operations, $P^6_{xyz} \otimes I^2_x \otimes I^2_y \otimes I^2_z$, that leave $\varepsilon(\mathbf{r})$ unchanged. For spheroids oriented in

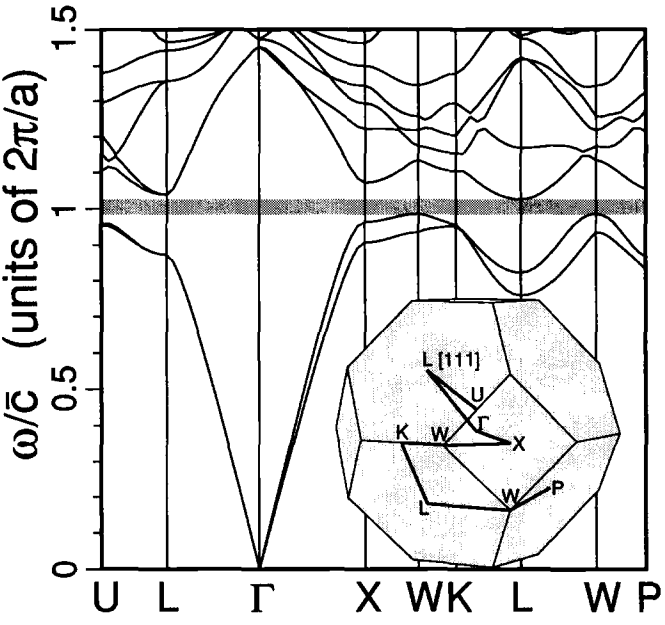


Figure 5. The band structure for prolate air spheroids oriented along the (111) direction in f.c.c. $\varepsilon_b=25$, $\varepsilon_a=1$, $\beta=\pi/6$, $\sigma_1=\sigma_2=\pi/2$, $\sigma_3=\pi$ and $\beta=\pi/6$. $\bar{c}\equiv c/\sqrt{\bar{\varepsilon}}$. Inset shows the path in the Brillouin zone. $P=(-3/8, 3/4, -3/8)$. Over 1400 plane waves were used for this calculation.

the (111) direction, this number is reduced to 12: $P^6_{xyz}\otimes I^2_r$. Here $P$ denotes permutation, $I$ denotes inversion and the superscripts are the multiplicities associated with each operation. Hence, the irreducible portion of the Brillouin zone is four times larger than that for spheres. One must traverse the edge of this region extensively when searching for gaps.

In figure 5 we plot the band structure for the case $\varepsilon_b=25$, $\varepsilon_a=1$, $\beta=\pi/6$, $\sigma_1=\sigma_2=\pi/2$, $\sigma_3=\pi$. Convergence of the **E** method is excellent for this case. We find that for $N=57$, 113, 341, 751 and 1419 the relative gap $\Delta_{23}$ is 2·72%, 3·8%, 3·89%, 3·95% and 3·98% of the centre frequency and extrapolates to $\sim$4·3% as $N^{-1/3}\to 0$. Using the **H** method, we obtain 2·29%, 9·19%, 9·9%, 9·27% and 8·35% for the 2–3 gap, and an extrapolation does not, at this point, yield a result consistent with that of the **E** method. However, a glance at the overall band structure obtained by each method as $N$ is increased leaves no doubt that the **E** method is far superior for this case. With $\varepsilon_b=13$, a similar analysis yields $\Delta_{23}\approx 2{\cdot}5\%$ as $N^{-1/3}\to 0$ for the first gap. $\beta=\pi/6$ is the maximum volume fraction for $\sigma_3/\sigma_{12}=2$ and each spheroid is in contact with six neighbours from the two adjacent (111) planes, instead of the 12 for the spherical close-packed case. With $\varepsilon_a$ fixed at 1, i.e. for air spheroids, we varied three parameters, $\varepsilon_b$, the aspect ratio $\sigma_1/\sigma_3$ and the volume fraction $\beta$ of spheroids, each time keeping the other two parameters constant.

In figure 6 we plot the relative 2–3 gap $\Delta_{23}$ against $\varepsilon_b$ with the same geometry as in figure 5. Not surprisingly, the gap increases with $\varepsilon_b$, but tends to level off. This is understandable since the relative ripple, $\|\varepsilon_r\|$, also approaches a constant value as $\varepsilon_b\to\infty$.

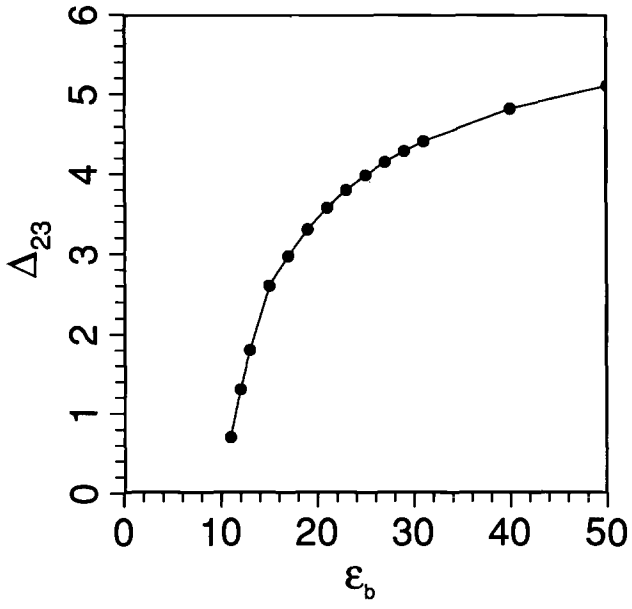


Figure 6. Relative 2–3 gap $\Delta_{23}$ against $\varepsilon_b$ for the geometry as in figure 5. Over 1300 plane waves were used for this calculation.

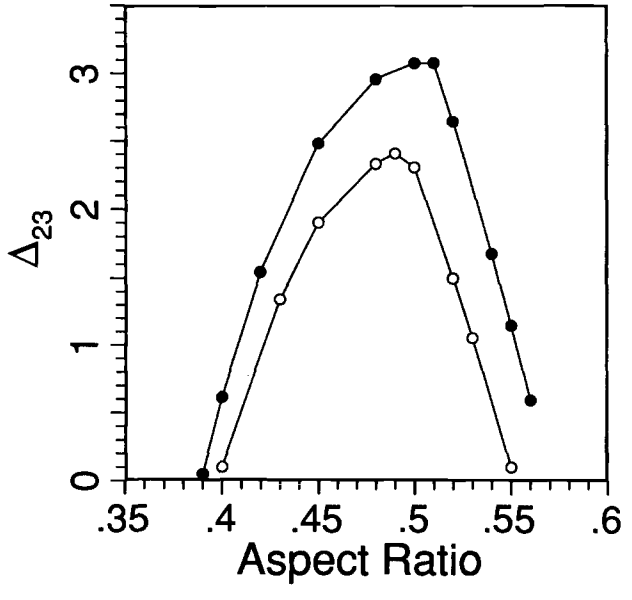


Figure 7. Relative 2–3 gap $\Delta_{23}$ against the aspect ratio $\sigma_1/\sigma_3$, with $\varepsilon_b = 25$ for $\beta = 0{\cdot}5$ (○) and $\beta = 0{\cdot}51$ (●). Spheroids are oriented along the (111) direction. Over 1300 plane waves were used for this calculation.

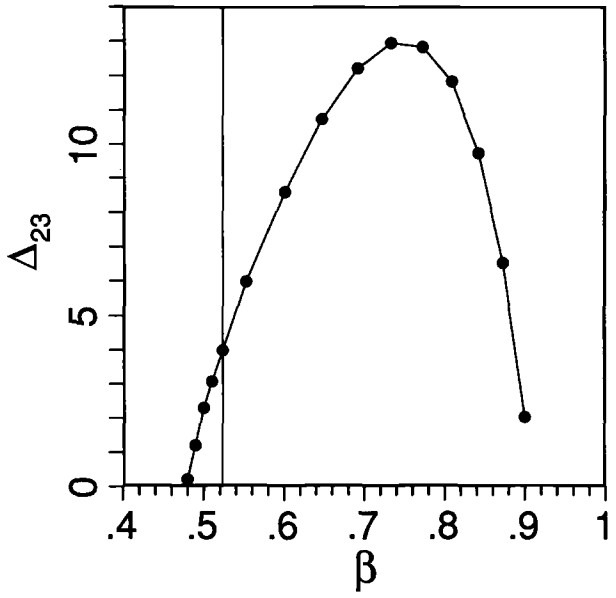


Figure 8. $\Delta_{23}$ against $\beta$ with $\varepsilon_b = 25$ and $\sigma_1/\sigma_3 = 0{\cdot}5$. Spheroids are oriented along the (111) direction. Over 1300 plane waves were used for this calculation. As $\beta$ is reduced from its close-packed value of $\pi/6$ (vertical line), the gaps are rapidly diminished. For $\beta > \pi/6$ the spheroids 'overlap'.

The relative gaps $\Delta_{23}$–$\Delta_{78}$ for various values of the FT grid size (→) and $N$, the number of plane waves (↓). All values are calculated with the **E** method.

| | $50 \times 50 \times 50$ | $100 \times 100 \times 100$ | $200 \times 200 \times 200$ | $400 \times 400 \times 400$ |
|---|---|---|---|---|
| 113 | 14·68–3·07 | 13·03–4·15 | 12·65–4·31 | 12·45–4·34 |
| 339 | 14·95–3·66 | 13·24–4·70 | 12·85–4·83 | 12·62–4·85 |
| 751 | 14·98–3·91 | 13·22–4·94 | 12·81–5·09 | 12·57–5·11† |
| 1450 | 15·00–4·11 | 13·22–5·15 | 12·80–5·33 | 12·56–5·36 |

† With the **H** method we obtain 10·96–6·8.

Figure 7 is a plot of $\Delta_{23}$ against the aspect ratio $\sigma_1/\sigma_3$, with $\varepsilon_b = 25$ and $\beta = 0{\cdot}5$ and $\beta = 0{\cdot}51$. Around $\sigma_1/\sigma_3 = 0{\cdot}5$ where the spheroids from two adjacent (111) planes come very close to touching, the gap, although small, has a sharp peak.

Figure 8 shows the dependence of $\Delta_{23}$ on $\beta$ with $\varepsilon_b = 25$ and $\sigma_1/\sigma_3 = 0{\cdot}5$. Reducing $\beta$ from its close packed value of $\pi/6$ rapidly diminishes the gaps. For $\beta > \pi/6$ the spheroids 'overlap'. For these cases $\varepsilon(\mathbf{r})$ cannot be written in the form of equation (22), but rather, more generally, as

$$\varepsilon(\mathbf{r}) = \begin{cases} \varepsilon_a, & \text{if } u(\mathbf{r}-\mathbf{R}) < 1, \quad \text{for any } \mathbf{R}, \\ \varepsilon_b, & \text{otherwise.} \end{cases} \tag{25}$$

The expression equation (23) for $\varepsilon(\mathbf{G})$ no longer holds for these structures. To calculate $\varepsilon(\mathbf{G})$, we divided the cube that contains the primitive f.c.c. Wigner–Seitz cell into a $200 \times 200 \times 200$ grid. The effect of grid size and $N$ on the calculated

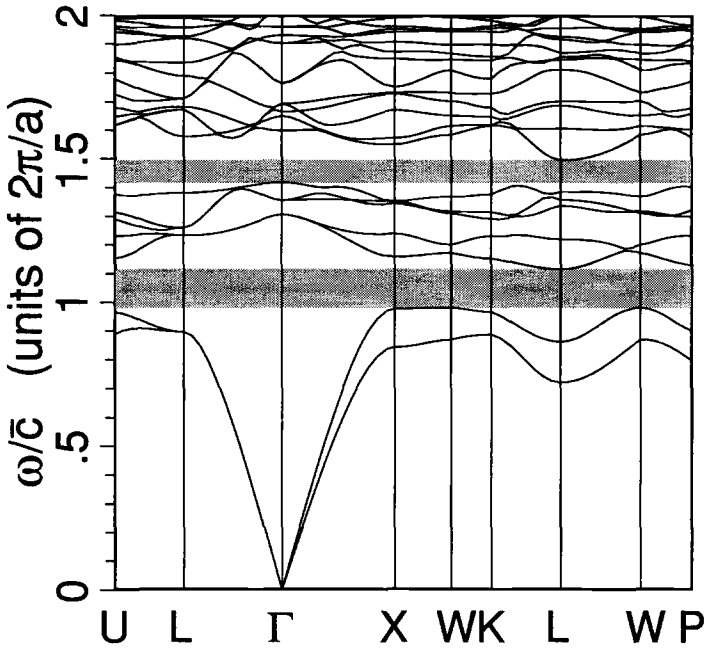


(*a*)

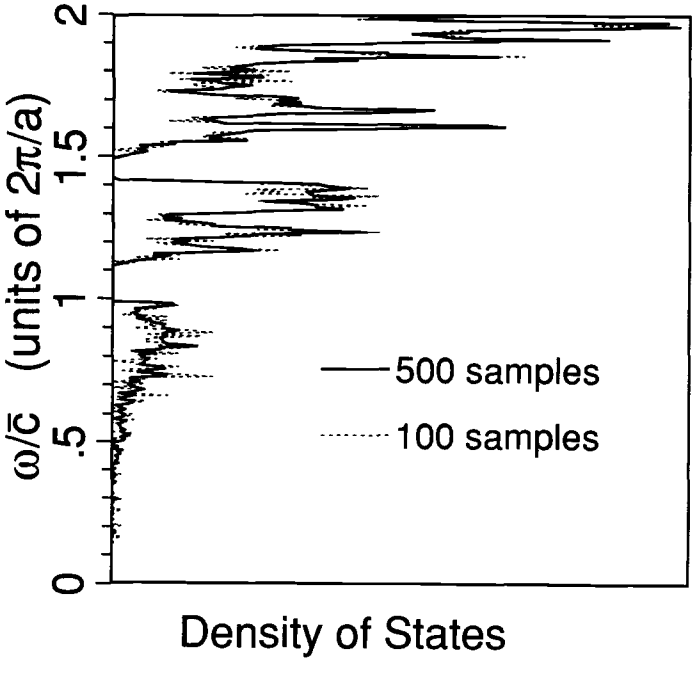


(*b*)

Figure 9. (*a*) The band structure for 'overlapping' prolate air spheroids oriented along the (111) direction in f.c.c. $\varepsilon_b = 25$, $\varepsilon_a = 1$, $\beta = 0{\cdot}77$, $\sigma_1 = \sigma_2 = \pi/2$, $\sigma_3 = \pi$ and $\beta = \pi/6$. Over 1400 plane waves used for this calculation. (*b*) The density of states for the same structure calculated with 100 (dotted) and 500 (solid) randomly selected **k** points in the Brillouin zone.

bandgaps is summarized in the table. With the **E** method, a coarse grid somewhat overestimates the 2–3 gap but underestimates the 7–8 gap. However, looking at the table, it is safe to say that the results are quite reliable. With the **H** method, however, a 200 × grid gives completely nonsensical results when a large number of plane waves are employed—a grim reminder, perhaps, that one is indeed walking on thin ice when using numerical Fourier transforms. This is indeed not surprising. For $N \approx 1500$, the matrix $\varepsilon(\mathbf{G}-\mathbf{G}')$ contains values with $|\mathbf{G}-\mathbf{G}'|$ up to about 22. For these Fourier components, using a 200 × grid corresponds to about ten samples per wavelength and this is further reduced by a factor of $\sqrt{3}$ when **G** is in the (111) direction. With a 400 × grid, however, we did manage to get meaningful—albeit still inaccurate—results with the **H** method: for the same structure as in figure 9, we obtain, using 750 plane waves, $\Delta_{23}=11\%$ and $\Delta_{78}=6{\cdot}8\%$. We also use a spherical, rather than an ellipsoidal truncation in **G** space for these structures, as $\varepsilon(\mathbf{G})$ no longer has ellipsoidal symmetry.

The 2–3 gap peaks to a value of $\sim 12\%$ around $\beta \sim 0{\cdot}75$. Moreover, a second gap opens between the seventh and eighth bands and peaks to $\sim 6\%$ around $\beta \sim 0{\cdot}81$. This gap is more difficult to interpret due to the complex geometry of the medium. The size of this gap is also less accurate, but the fact that it *increases* as the grid size and $N$ is increased suggests that it is not a numerical artifact (see the table). Figure 9 (*a*) is the band structure at $\beta=0{\cdot}77$, where $\Delta_{23}$ peaks. Figure 9 (*b*) shows the density of states calculated from a random sample of 500 **k** points in the Brillouin zone. The jagged appearance is due to poor statistics for small **k**. The dotted curve is the density of states calculated with only 100 samples for comparison.

It is interesting to note that the topology of this medium is identical to that of the structure reported in [2], i.e. circular rods along the (011), (101) and (110) directions in f.c.c. In fact we found that a similar dielectric scaffold structure in the simple cubic lattice, rods with a square cross-section along the cartesian axes, also yields large gaps [15]. Interestingly, the same structure in body centred cubic (b.c.c.) where one has two interlaced but disconnected scaffolds, did not yield gaps.



## 5. Conclusion

It was proposed earlier [1, 3] that the f.c.c. lattice would be ideal for a photonic bandgap to form because its Brillouin zone is closest to a sphere. However, in view of the degeneracy of the second and third bands with spherical atoms, it was later conjectured [2] that a microstructure with non-spherical atoms would lift the degeneracy and yield bandgaps. However, we found that the same degeneracy persists with cubic atoms. While we are far from a precise definition of the conditions that would yield such gaps, we believe our findings, coupled with various other studies, suggest that the f.c.c. lattice in not necessarily special and that the emergence of gaps seems to be related to the strength of the dielectric modulation [10] and to the connectivity of the *a* and *b*-type materials. For example, with spheroids oriented along the (100) and (110) directions, the *a*-type material cannot be made to be connected throughout the crystal. The most one gets, by varying the aspect ratio, are either 'cylinders' or 'planes' that are disjoint, and these structures did not possess gaps. The small gap which opens just before the spheroids come into contact is real and can loosely be interpreted as a capacitive/inductive effect or as barrier penetration, since the spheroids are barely separated from each other.

We also find that the analytical criteria suggested by John [17], $\beta_0 = \frac{1}{2}(\varepsilon_a/\varepsilon_b)^{1/2}$, and the authors [10], $\beta_0 = \varepsilon_b/(\varepsilon_b + \varepsilon_a)$, for the optimum value of $\beta$ that maximizes the gaps do not fare too well. The former is based on the requirement that the Bragg and the Mie resonances occur at the same frequency for a one-dimensional medium, and yields $\beta_0 = 0{\cdot}9$ for a dielectric contrast of 25. Ours is derived by maximizing $\|\varepsilon_r\|$ and yields $\beta_0 = 0{\cdot}96$. We find the peak of the 2–3 gap around $\beta_0 = 0{\cdot}75$. Clearly, it is indeed somewhat naïve to expect that any simple formula could explain a phenomenon as complicated as the band structure. These are guidelines and should not be viewed simplistically.

We have shown that there can exist multiple gaps which can be exploited in a number of novel applications where blocking multi-channel spontaneous emissions may be necessary. The second gap also eases the restriction on the lattice constant required to match the bandgap to the required frequency.

We have shown that $\varepsilon_{\text{eff}}$ depends very critically on geometry for densely packed particles and that theories that attempt to describe $\varepsilon_{\text{ff}}$ without regard to geometry are at best approximate in this regime.

There still remains the problem of convergence which we have partially overcome by an extrapolation to an infinite number of plane waves and using the two method described. However, even this extrapolation scheme fails to be consistent in many cases of interest [10]. Clearly, a graded dielectric function, such as a Gaussian, yields much faster convergence. Another possibility is to use multiple dielectric coatings or doping the particles during growth. Our test calculations with dielectric spheres with a single layer of coating of dielectric constant between $\varepsilon_a$ and $\varepsilon_b$, indicate a vastly improved convergence. Furthermore, in view of the fact that we have obtained large gaps with Gaussian spheres in the diamond structure [10], there is reason to believe that such a coating would enhance the gaps.

Finally, we recognize the need for using alternate methods, such as the augmented plane wave (APW) or Korringa, Kohn and Rostoker (KKR), which may be expected to converge faster. However, these methods are limited largely to spherical atoms, and are quite cumbersome from a computational point of view.



## Acknowledgments

We thank the authors of [2] and [6] for providing us with the preprints of their papers. This work was supported by the National Science Foundation Grant No. ECS-8813028 and J.W.H. was supported by the DARPA funded Optoelectronics Technology Center. The computations were performed on the IBM 3090-200S Vector Facility at the Voorhees Computing Center at RPI and on the IBM 3090-600J at the Cornell National Supercomputing Facility.

## References

[1] YABLONOVITCH, E., 1987, *Phys. Rev. Lett.*, **58,** 2059; YABLONOVITCH, E., and GMITTER, T. J., 1989, *Phys. Rev. Lett.*, **63,** 1950.
[2] YABLONOVITCH, E., and LEUNG, K. M., 1991, *Physica* B, **175,** 81.
[3] JOHN, S., 1987, *Phys. Rev. Lett.*, **58,** 2486.
[4] ECONOMOU, E. N., and ZDETSIS, A., 1989, *Phys. Rev.* B, **40,** 1334; LEUNG, K. M., and LIU, Y. F., 1990, *Phys. Rev. Lett.*, **65,** 2646; ZHANG, Z., and SATPATHY, S., 1990, *Phys. Rev. Lett.*, **65,** 2650.
[5] HO, K. M., CHAN, C. T., and SOUKOULIS, C. M., 1990, *Phys. Rev. Lett.*, **65,** 3152.

[6] YABLONOVITCH, E., GMITTER, T. J., MEADE, R. D., RAPPE, A. M., BROMMER, K. D., and JOANNOPOULOS, J. D., 1991, *Phys. Rev. Lett.*, **67,** 3380.
[7] YOKOYAMA, H., and BRORSON, S. D., 1989, *J. Appl. Phys.*, **66,** 4801; YAMAUCHI, T., ARAKAWA, Y., and NISHIOKA, N., 1991, *Appl. Phys. Lett.*, **58,** 2239.
[8] SÖZÜER, H. S., and HAUS, J. W., 1991, unpublished.
[9] KURIZKI, G., and GENACK, A. Z., 1988, *Phys. Rev. Lett.*, **61,** 2269; KURIZKI, G., 1988, *Phys. Rev.* A, **42,** 2915; ADLER, C. L., and LAWANDY, N. M., 1991, *Phys. Rev. Lett.*, **66,** 2617; JOHN, S., and WANG, J., 1990, *Phys. Rev. Lett.*, **64,** 2418.
[10] SÖZÜER, H. S., HAUS, J. W., and INGUVA, RAMARAO, 1992, *Phys. Rev.* B, **45,** 13962.
[11] SÖZÜER, H. S., HAUS, J. W., and INGUVA, RAMARAO, 1992, unpublished.
[12] BERTHIER, S., 1988, *Ann. Phys.* (*Paris*), **13,** 503.
[13] HAUS, J. W., KALYANIWALLA, N., INGUVA, R., BLOEMER, M., and BOWDEN, C. M., 1989, *J. opt. Soc. Am.* B, **6,** 797.
[14] LAMB, W., WOOD, D. M., and ASHCROFT, N. W., 1980, *Phys. Rev.* B, **21,** 2248.
[15] SÖZÜER, H. S., and HAUS, J. W., 1992, *J. opt. Soc. Am.* B, submitted for publication.
[16] GLAUBER, R. J., and LEWENSTEIN, M., 1991, *Phys. Rev.* A, **43,** 467.
[17] JOHN, S., 1991, *Physics Today*, May, p. 32.